The iron-dopamine D1 coupling modulates neural signatures of working memory across adulthood

Jonatan Gustavsson[1], Jarkko Johansson[2], Farshad Falahati[1], Micael Andersson[4], Goran Papenberg[1], Bárbara Avelar-Pereira[1], Lars Bäckman[1], Grégoria Kalpouzos*[1], Alireza Salami*[1,3,4]

[1]Aging Research Center, Karolinska Institutet and Stockholm University, Sweden. [2]Umeå University, Faculty of Medicine, Department of Radiation Sciences, Sweden. [3]Wallenberg Center for Molecular Medicine at Umeå University [4] Department of Integrative Medical Biology, Umeå University, Umeå, Sweden

*Authors share the position as last authors.

1 Abstract

Brain iron overload and decreased integrity of the dopaminergic system have been independently reported as brain substrates of cognitive decline in aging. Dopamine (DA), and iron are co-localized in high concentrations in the striatum and prefrontal cortex (PFC), but follow opposing age-related trajectories across the lifespan. DA contributes to cellular iron homeostasis and the activation of D1-like DA receptors (D1DR) alleviates oxidative stress-induced inflammatory responses, suggesting a mutual interaction between these two fundamental components. Still, a direct in-vivo study testing the iron-D1DR relationship and their interactions on brain function and cognition across the lifespan is rare. Using PET and MRI data from the DyNAMiC study (n=180, age=20-79, %50 female), we showed that elevated iron content was related to lower D1DRs in DLPFC, but not in striatum, suggesting that dopamine-rich regions are less susceptible to elevated iron. Critically, older individuals with elevated iron and lower D1DR exhibited less frontoparietal activations during the most demanding task, which in turn was related to poorer working-memory performance. Together, our findings suggest that the combination of elevated iron load and reduced D1DR contribute to disturbed PFC-related circuits in older age, and thus may be targeted as two modifiable factors for future intervention.

Keywords: Dopamine, Iron, Working memory, Age, BOLD

2 Introduction

Aging is associated with cognitive decline (Gorbach et al., 2017; Salthouse, 2012) and concomitant alterations in structural, functional, and molecular properties of the brain (Andrews-Hanna et al., 2007; Bäckman et al., 2000; Gorbach et al., 2017; Zimmerman et al., 2006). Elevated iron content and decreased integrity of the dopaminergic system are typically reported as independent brain substrates of age-related cognitive decline (Bäckman et al., 2006, 2011; Cools & D'Esposito, 2011; Daugherty et al., 2015; Gustavsson et al., 2022; Hallgren & Sourander, 1958; Kalpouzos, 2018; Landau et al., 2009; Nyberg, Andersson, et al., 2009; Salami et al., 2019). Intracellular non-heme iron is involved in several fundamental neurobiological processes, including dopamine (DA) metabolism (Hare & Double, 2016;

Mills et al., 2010). More specifically, iron is a cofactor of tyrosine hydroxylase during DA synthesis, indicating a critical role of iron in DA metabolism as well as in the development of the dopaminergic system (Erikson et al., 2001; Ortega et al., 2007; Unger et al., 2014; Zucca et al., 2017).

Iron is stored in the ferritin protein which keeps it from harming brain cells and is released upon metabolic demand. However, unbound iron accumulates with advancing aging and exerts detrimental effects on cellular integrity. Elevated iron content contributes to poorer myelin integrity (Steiger et al., 2016) and grey-matter atrophy (Daugherty & Raz, 2015, 2016), as well as altered frontostriatal activity (Kalpouzos et al., 2017; Rodrigue et al., 2020; Salami et al., 2021) along with disrupted functional connectivity in aging (Salami et al., 2018). Similar to consequences of elevated iron in aging, disruption of the DA system contributes to age-related neurocognitive impairment (Bäckman et al., 2006, 2011; Cools & D'Esposito, 2011; Landau et al., 2009; Nyberg, Dahlin, et al., 2009; Rieckmann et al., 2011; Salami et al., 2019). Given DA and iron are co-localized in high concentrations in the striatum, age-related iron dyshomeostasis combined with disturbance of the DA system may become harmful for brain integrity and cognition. Direct in-vivo studies testing the synergistic effects between the dopaminergic system and iron on brain function and cognition in aging are rare.

Past studies suggest that iron may cause neurotoxicity through DA oxidation, which may in turn contribute to loss of dopaminergic neurons (Hald & Lotharius, 2005; Hare & Double, 2016; Youdim et al., 1993; Zucca et al., 2017). Animal studies have demonstrated that iron-induced damage causing DA depletion (Poetini et al., 2018) and deterioration of dopaminergic cells (Kaur et al., 2003) could be restored after iron chelation. In contrast, a longitudinal study showed that dopaminergic cell death precedes iron elevation in parkinsonian monkey (He et al., 2003). A study with young, middle-aged, and older rhesus monkeys reported an association between iron and stimulus-evoked levels of DA (Cass et al., 2007), with older monkeys exhibiting more iron accumulation and less DA release. Although it remains unclear whether elevated iron is the cause or consequence of DA degeneration, it

is relatively well acknowledged in animal studies that these two key chemical components of the brain interact with each other (Hare & Double, 2016).

As opposed to ample animal studies on iron-DA coupling, evidence for such an association across the adult lifespan in humans is scarce. A recent longitudinal study showed that developmental changes in pre-synaptic, but not post-synaptic, DA receptors were positively associated with iron accumulation through adolescence and young adulthood (Larsen et al., 2020). Still, iron and DA play ambivalent roles during early and later adulthood (Johansson et al., 2022; Kalpouzos et al., 2017; Salami et al., 2021). Recent work showed that older individuals with genetic predisposition for lower DA (by proxy of the *COMT* Val158Met genetic polymorphism) accumulated more iron in the dorsolateral prefrontal cortex (DLPFC) and striatum over 3 years (Gustavsson et al., 2022). Postsynaptic DA markers, particularly DA D1-like receptor (D1DRs) which are the most abundantly expressed receptor subtypes, are among the most age-sensitive DA systems (Karrer et al., 2019). Moreover, the activation of D1 and D2 receptors alleviates oxidative stress-induced inflammatory responses (Shao et al., 2013; Yan et al., 2015; Zhu et al., 2018). Hence, with diminished DADRs, the capacity of the protective response counteracting oxidative stress and neuroinflammation due to iron overload is lessened, and may lead to increased damage and ferroptosis (Hald & Lotharius, 2005).

Motivated by the lack of human studies, we investigated the relationship between dopaminergic receptors and iron content, and their interactions on brain function and cognition. Using the largest D1DR dataset across the world, we studied 180 healthy individuals (20-79 years old) who underwent D1DR Positron Emission Tomography (PET) assessment using [^{11}C]SCH23390, iron approximation made with magnetic resonance imaging (MRI) based quantitative susceptibility mapping (QSM; (Langkammer et al., 2012)), and functional magnetic resonance imaging (fMRI) while performing a working-memory task. We first examined regional variation in the link between D1DR and iron content with the hypothesis that greater iron content is related to lower D1DR, with a possible interaction with age (C.f. Salami et al., 2021; Kalpouzos et al.,2018). We targeted DLPFC and striatum, because of

abundantly expressed D1DR (Shohamy & Adcock, 2010), pronounced age-related D1DR differences (Karrer et al., 2017), and association between *COMT* polymorphism (i.e., a dopaminergic gene) and iron accumulation reported in these regions (Gustavsson et al., 2022). Given the association of iron and DA to neural circuits of working memory (c.f., Salami et al., 2021; Salami et al., 2019), we predicted an interactive effect of iron and D1DR on load-dependent BOLD modulation and working memory processing (Gustavsson et al., 2022; Spence et al., 2020). To this end, we applied multivariate partial-least squares (PLS; ((McIntosh & Lobaugh, 2004)) which enables a simultaneous analysis of iron content, D1DR, age, on BOLD associations across all task conditions in a data-driven fashion. If these variables are simultaneously related to neural circuits of WM, PLS should reveal a single network showing that older individuals with elevated iron and decreased D1DR (i.e., toxic iron-DA coupling) exhibit lower task-related BOLD-response, particularly within the frontoparietal network. However, if D1DR and iron differentially modulate BOLD response (c.f., Salami et al., 2019; Salami et al., 2021), PLS should reveal different networks.

2. Results

2.1 Demographics.

Demographic information along with data on body mass index (BMI), brain volumes, D1DR, and N-back performance are presented in Table 1.

Table 1. Participant characteristics

		Mean	SD
N (Women)	162 (79)		
Age		50	17
Age range		20-78	
MMSE		28.8	1.1
BMI		25.2	3.9
Education		15	3.4
Volume[a]			
DLPFC		20478	2696
Striatum		11473	1282
Iron [b]			
DLPFC		0.0430	0.0140
Striatum		0.0998	0.0286
D1DR			
DLPFC		0.3582	0.0690
Striatum		1.6130	0.2182
WM performance			
1-back accuracy[c]		75.18	6.65
1-back (H-FA)[d]		0.86	
2-back accuracy		60.99	8.77
2-back (H-FA)		0.72	
3-back accuracy		48.10	9.57
3-back (H-FA)		0.59	

Note. MMSE = Mini Mental State Examination,
DLPFC = Dorsolateral prefrontal cortex, SD = Standard deviation.
[a] Volume (mL) adjusted for total intracranial volume
[b] Approximation of iron, based on susceptibility in parts per million
[c] Accuracy calculated as the sum of correct responses
[d] Proportion of false alarms (FA) subtracted from proportion of hits (H)

The MANCOVA conducted on N-Back performance showed a significant main effect on load conditions ($F_{2,155}$ = 228.24, $p < 0.001$, Wilk's Λ = 0.253, partial η^2 = 0.747), and an age-group effect on load conditions ($F_{4,310}$ = 9.43, $p < 0.001$, Wilk's Λ = 0.795, partial η^2 = 0.108). Post-hoc analysis for the lowest WM load (1-back) showed that the older participants performed less accurately compared to both middle-aged (t_{89} = -3.974, $p < 0.001$) and younger participants (t_{71} = -5.707, $p < 0.001$). There was no significant difference between younger and middle-aged participants (p = 0.07). For 2-back, older participants performed significantly poorer compared to both middle-aged (t_{105} = -4.015, $p < 0.001$) and younger participants (t_{85} = -8.905, $p < 0.001$). Middle-aged participants performed significantly

poorer compared to younger participants (t_{98} = -4.176, p < 0.001). Lastly, for highest WM load (3-back), older participants performed significantly poorer compared to both middle-aged (t_{105} = -5.300 p < 0.001) and younger participants (t_{102} = -7.950, p < 0.001). Middle-aged participants performed significantly poorer compared to younger participants (t_{105} = -2.921, p = 0.004).

2.2 Iron content in DLPFC, but not in striatum, was negatively associated with D1DR

Both striatal and DLPFC iron increased with advancing age (striatum: r = 0.551, p < 0.001; DLPFC: r = 0.244, p = 0.002). D1DRs in both regions decreased with advancing age (striatum: r = -0.62, p < 0.001; DLPFC: r = -0.565, p = < 0.001).

The partial correlation analysis for iron content and D1DR in DLPFC showed a significant negative association across the whole sample (r = -0.272, p < 0.001), suggesting that greater iron content was linked to lower D1DR (Fig. 1B). Further group level analyses revealed that this correlation was similarly expressed across different age groups (Younger: r = -0.10, p = 0.48; Middle-aged: r = -0.30, p = 0.026; Older: r = -0.37, p = 0.006). However, striatal iron content was unrelated to D1DR across the whole sample (r = -0.101, p = 0.20; supplementary materials, Fig. 1B). No significant association was observed within each age groups (Ps > 0.05), except for a trend-level link in the older individuals (r = -0.24, p = 0.08).

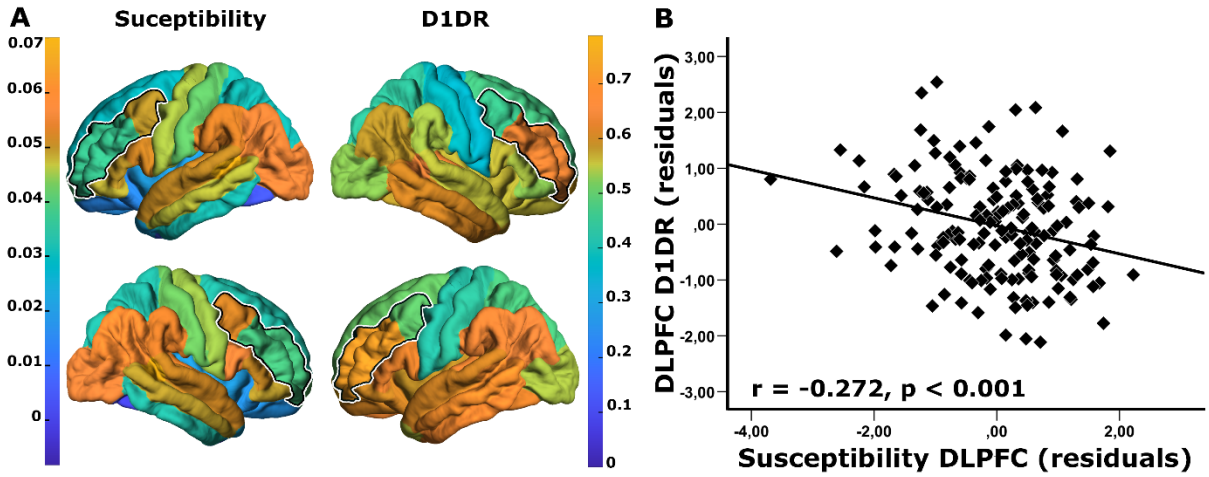

Figure 1. The relationship between iron content and D1DR in dorsolateral prefrontal cortex. **(A)** Surface map representing distribution of cortical iron (susceptibility in parts per million; left column) and D1DR ([^{11}C]SCH23390 BP_{ND}; right column) with dorsolateral prefrontal cortex (DLPFC) outlined. **(B)** Scatterplot depicting the association between greater iron content and lower D1DR in DLPFC. All values are z-transformed residuals adjusting for age.

2.3 Iron-D1DR couplings in DLPFC modulates WM-related BOLD in a load-dependent fashion

Given the iron-D1DR link in DLPFC, we next investigated whether iron-D1DR coupling modulated neural correlates of PFC-related function across the adult lifespan. We used behavioural PLS to assess the presence of multivariate spatial patterns of task-related BOLD response dependent on age, iron content, and D1DR across load conditions during N-back working memory task. The analysis identified two significant latent variables (LVs). LV1 represented a brain-wide network with increased activation in older individuals in a load-independent fashion. This network was largely unrelated to D1DR or iron in DLPFC (supplementary materials 5.1.2, Table 1, Fig 2).

The second LV represented the canonical WM network (c.f. Nagel et al., 2009; Salami et al., 2018). This LV (permuted p = 0.02, 17.97% of cross-block covariance: Fig. 3A) demonstrated that older individuals with elevated iron content and lower D1DR in DLPFC exhibited lower BOLD response in the frontoparietal network during 3-back (Fig. 3B). In contrast, higher BOLD response in the frontoparietal

network during 1-back was associated with older age and lower D1DR in DLPFC, but not with iron content. For 2-back, no associations were considered reliable as the CI:s overlapped with zero (Fig. 3B). As opposed to the frontoparietal WM network, the default-mode network (Fig. 3A (Blue areas); supplementary Table 2) was less deactivated during 3-back in older individuals with higher iron content and lower D1DR in DLPFC. Taken together, these results revealed that iron-D1DR coupling modulates neural correlates of the working memory in a load-dependent fashion.

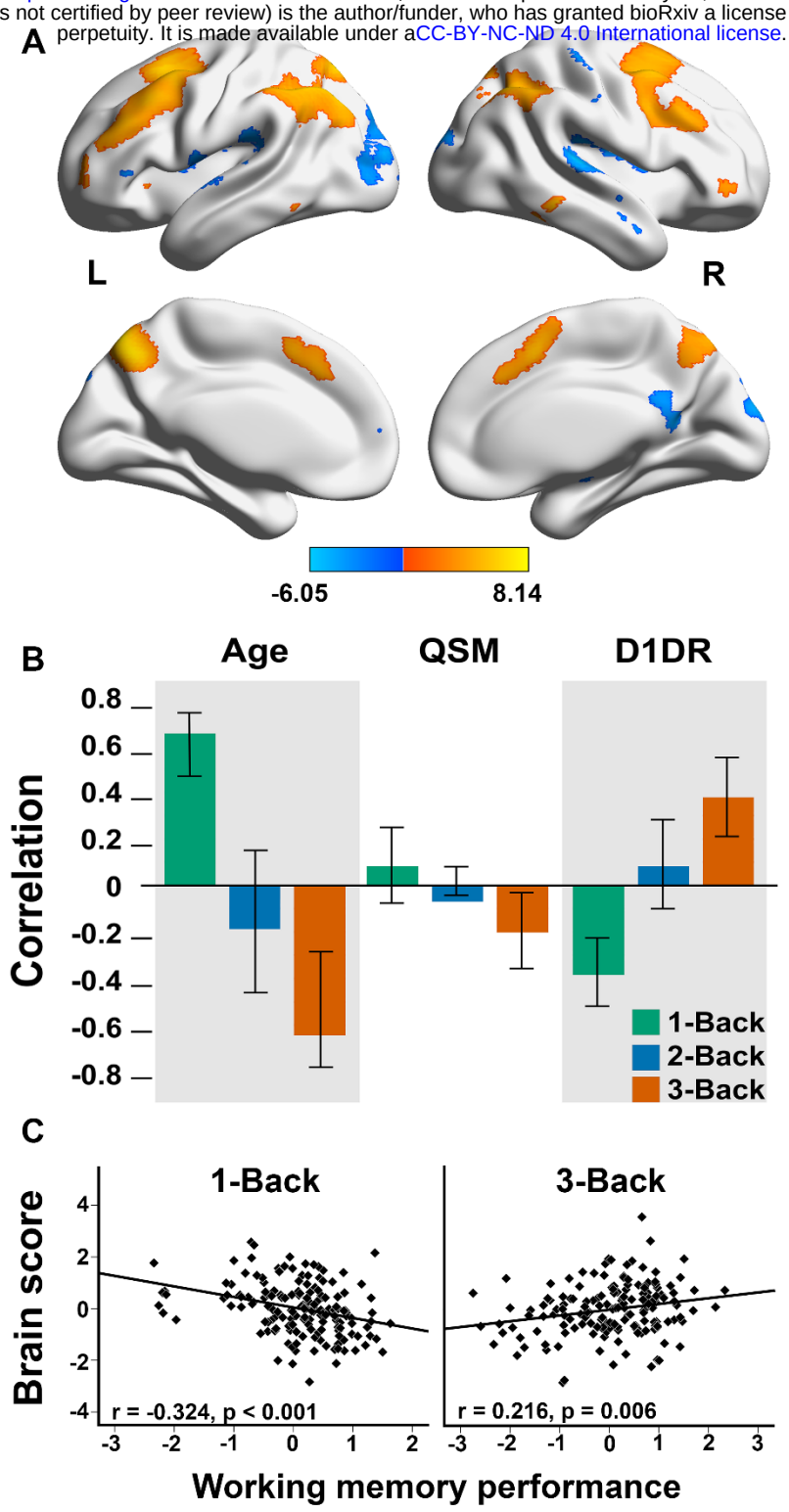

Figure 3. Multivariate relationship of BOLD response patterns during working-memory task identified by task PLS. **A)** The regions depicted in a yellow colour mainly correspond to the frontoparietal network, whereas the blue colour mainly represents the default-mode network. The frontoparietal network showed greater activation in correspondence to the behavioural measures across different task conditions, whereas the default-mode network showed greater deactivation (i.e., less activation). **B)** BOLD association across age, iron content (QSM), and D1DR. Interpretation of the figure should be as reliable positive and negative associations of activation (BOLD response) when the confidence intervals (CI:s) do not overlap with zero. As the frontoparietal network displayed increased activation, a positive association is interpreted as greater activation, whereas a negative

association is interpreted as less activation. For the default-mode network the opposite applies. **C)** Greater activation was associated with poorer performance during 1-back, but greater performance during 3-back. All values are z-transformed residuals adjusting for age.

2.4 Load-dependent BOLD response is differentially associated with task performance.

We have shown that increasing age was concomitant with increased and decreased activations within the frontoparietal network during 1-back and 3-back, respectively. We next tested the relationship of brain activation in relation to task performance. The brain score during 1-back was negatively associated with 1-back performance ($r = -0.324$, $p < 0.001$; Fig. 3C), but positively with 3-back ($r = 0.216$, $p = 0.006$; Fig. 3C). No significant association was observed during 2-back ($r = 0.05$, $p=0.4$). Taken together, our results suggest that less frontoparietal activity during 3-back as well as greater frontoparietal activity during 1-back are associated with less efficient working memory function.

2.5 Control analyses

To confirm that the results obtained from the partial correlation analyses were not due to confounding variables, we performed additional analyses in which we controlled for sex, education, and regional grey-matter volume. The inclusion of the additional variables did not result in a noticeable change of the outcome and all the patterns remained consistent. A full description of the results is given in the supplementary results.

3. Discussion

In this study, we provide first in-vivo evidence for an association between D1DR and brain iron across the adult lifespan, and how iron-D1DR synergy may contribute to disturbed brain responses during WM task performance across the lifespan. The main findings were that greater iron content was associated with lower D1DR in DLPFC, but not in striatum, across the adult lifespan. We also found that older individuals with elevated iron content and lower D1DR in DLPFC – a presumably deleterious synergy – exhibited lower frontoparietal activity along with less deactivation of the DMN during high

demand condition and in turn poorer WM performance. Although the associations revealed by these data are cross-sectional, a plausible interpretation is that elevated iron and lower D1DR together form a toxic couple (c.f. Hare & Double, 2016), which would contribute to reduced network dynamics and impaired WM processing.

A key finding of the present study is the association between higher iron content and lower D1DR in DLPFC across the adult lifespan. The exact mechanism underlying the association between iron content and DA receptors is poorly understood. The dopaminergic system is important to cellular iron homeostasis, as documented in *in vitro* studies (Dichtl et al., 2018; Liu et al., 2021). Supporting this idea, we recently demonstrated that older adults with genetic predisposition for lower DA levels accumulated more iron in DLPFC and striatum over time compared to individuals with presumably higher DA levels (Gustavsson et al., 2022). Age-related differences in pre- and postsynaptic DA markers (Bäckman et al., 2006, 2010) may also contribute to iron dyshomeostasis in aging, resulting in disruption of transportation of iron via transferrin and storage in the ferritin protein (Ward et al., 2014). Disruption of iron handling may lead to increase of ferrous iron, which triggers oxidative stress, neuroinflammation, and cell loss due to ferroptosis (Daugherty et al., 2015; Mazhar et al., 2021; Salami et al., 2021). The activation of D1 and D2/3 receptors alleviates oxidative stress-induced inflammatory responses (Shao et al., 2013; Yan et al., 2015; Zhu et al., 2018). However, whether age-related loss of DA receptors leads to an iron-related increase of oxidative stress and ferroptosis, or whether an age-related increase of iron causes loss of DA receptor cells can only be determined in a longitudinal setting.

We did not observe any significant association between iron and D1DR in striatum, except for a trend-level negative association in older age. The reason for these regional variations is unclear. One possibility is that, as D1DR are more expressed in striatum compared to cortex (Shohamy & Adcock, 2010), striatal regions are less vulnerable or better at attenuating the damage from higher iron content. If too many receptors diminishes, or the threshold of the capacity for dealing with oxidative

stress is exceeded, the iron-induced damage to the cells may lead to ferroptosis (Lillig et al., 2008). This concords well with Parkinson's Disease studies reporting regional variations in synuclein pathology despite brain-wide iron accumulation (McCann et al., 2016), suggesting that additional factors may contribute to iron serving a pathological role.

The multivariate PLS analysis revealed that in older age the combination of higher iron and lower D1DR within DLPFC was related to high frontoparietal recruitment during low-demanding tasks along with weak frontoparietal upregulation at higher task demand, which in turn was associated with poorer working memory performance. These results concord with the Compensation-Related Utilization of Neural Circuits Hypothesis (CRUNCH; (Cappell et al., 2010; Mattay et al., 2006; Nyberg et al., 2014; Reuter-Lorenz & Cappell, 2008; Schneider-Garces et al., 2010)), which postulates that neural activity increases at low demanding task-levels in older adults compared to younger adults, but is reduced at more demanding levels.

The unique and shared contributions of iron content and neuroinflammation to astrocytic dysfunction in the neurovascular coupling has been proposed to account for the reduced BOLD response (Kalpouzos et al., 2017; Salami et al., 2018, 2021). Higher iron content has been related to inflammation (Haider, 2015; Salami et al., 2021), which can be detrimental to cells during prolonged periods (Hald & Lotharius, 2005; Zecca et al., 2004), thus contributing to astrocytic dysfunction. In vitro studies have demonstrated that DA receptors activation may alleviate and supress neuroinflammation (Liu et al., 2021; Shao et al., 2013; Yan et al., 2015). A more efficient dopaminergic system (e.g., manifested by greater receptor availability) protect against negative effects of iron and neuroinflammation on brain function. In support of this notion, a past study showed that age-related D1DR alteration alone may contribute to less efficient engagement of working memory circuits (Bäckman et al., 2011). Relatedly, the importance of DA for the frontoparietal BOLD response has been further demonstrated through pharmacological administration of a dopaminergic antagonist, leading to poorer working-memory performance (Fischer et al., 2010). Our results add novel contribution to the previous work, by showing

that the combination of elevated iron and D1DR reduction in DLPFC in aging, possibly reflecting synergistic iron-D1DR effects, exerts a deleterious effect in neural circuits of WM. Furthermore, during the most demanding WM condition (3-back), lower activation in the frontoparietal network was related to worse performance, in concordance with previous reports (Salami et al., 2021). Longitudinal data are needed to identify the primary mechanism of disturbed working memory circuit in older age.

Our study is the first to link regional iron content to DA receptor availability, by showing that greater iron content is related to lower D1DR. Critically, an interplay between age-related elevated iron content and diminished D1 receptor availability may provide a mechanistic understanding of how iron-DA coupling may exert deleterious effects on neural function and ultimately cognition. Elevated brain iron has been implicated in several neurodegenerative disorders, including Parkinson's disease, which is characterized by loss of dopaminergic cells (Ward et al., 2014). Thus, the observed findings have implications for better understanding the mechanisms behind DA-related neurodegeneration.

4 Materials and methods

This study uses data from the DopamiNe Age Connectome Cognition (DyNAMiC) project approved by the Umeå University Regional Ethical Board. All participants signed informed consent prior to data collection (for details about DyNAMiC, see Nordin et al., 2022).

4.1 Participants

One-hundred and eighty adults (mean age 49.8 ± 17.4 years; range 20-78; 90 females) from Umeå, Sweden, were recruited to participate in the project and underwent the full protocol, including cognitive testing, MRI, and PET assessments. All participants were native Swedish speakers, right-handed, and had no history of neurological illnesses. Of the sample of 180 participants, 3 dropped out of PET scanning, 4 were excluded due to incidental brain abnormalities, 3 due to failed reconstruction of QSM images. Additionally, brain and behavioural data were screened for univariate and multivariate outliers. Univariate outliers were defined as values greater or less than 3.29 SD from the mean (Tabachnick & Fidell, 2013) and excluded as pairwise deletions per ROIs and modality. Multivariate

289 outliers were identified according to Mahalanobis distance ($p < 0.001$; Tabachnick & Fidell, 2013). As a
290 result, five participants were identified as univariate outliers on their iron (n=3) or D1DR (n=2) values,
291 and three were multivariate outliers. Thus, data from 162 individuals were used in the analyses
292 involving iron content and D1D1R. Furthermore, three outliers were identified based on their online
293 WM performance and excluded from analyses.

294 **4.2 Neuroimaging acquisition and preprocessing**

295 Participants underwent positron emission tomography on a Discovery 690 PET/CT scanner (General
296 Electric) and MRI on a Discovery MR750 3.0 T scanner (General Electric) equipped with a 32-channel
297 phased-array head coil at two separate occasions at Umeå University Hospital.

298 *PET acquisition.* PET was conducted to assess whole-brain D1DR using radioligand [^{11}C]SCH23390 at
299 rest (for details see Nordin et al., 2022). The scanning session started with a low-dose CT image,
300 followed by an intravenous bolus injection of the radioligand. Participants were instructed to lay still
301 and stay awake with eyes open. An individually fitted thermoplastic mask was attached to the bed
302 surface during scanning to minimize head movement.

303 *Structural MR acquisition.* High-resolution anatomical T1-weighted images were acquired using 3D
304 fast-spoiled gradient echo sequence with the following parameters: 176 sagittal slices, slice thickness
305 = 1 mm, voxel size 0.49 x 0.49 x 1 mm^3, repetition time (TR) = 8.2 ms, echo time (TE) = 3.2 ms, flip angle
306 = 12°, field of view (FOV) = 250 x 250 mm, no spacing.

307 *Iron acquisition.* Images for iron estimation was obtained using a 3D multi-echo gradient-recalled echo
308 sequence (meGRE). The parameters were as follows: 124 axial slices, voxel size 1 x 1 x 1.2 mm^3, TR =
309 31 ms, flip angle = 17°, FOV = 256 x 256 mm, no spacing. The first TE was 1.78 ms followed by seven
310 additional TEs with a 2.87 ms interval.

311 *Functional MR acquisition*. The functional images were sampled using single-shot multiband EPI
312 sequence with 37 axial slices, voxel size 1.95 x 1.95 x 3.9 mm^3, 0.5 mm spacing, TR = 2.000 ms, TE = 30

ms, flip angle = 80°, and FOV = 250 × 250 mm. Ten dummy scans were collected at the start of the sequence.

In-scanner working memory task. A numerical N-back task was administered in the scanner (Salami et al., 2018). A sequence of single numbers appeared on the screen for 1.5s, with an interstimulus interval of 0.5s. During every item presentation, subjects indicated whether the digit on the screen was the same as the one shown 1, 2, or 3 digits back by pressing one of the two adjacent buttons with the index (Yes response) or middle finger (No response). Each working-memory load condition (1-, 2-, and 3-back) was presented over nine blocks in random order (interblock interval, 22 s) with each block consisting of 10 trials. For every block, 10 trials were performed with four matches (requiring a "yes" response) and six nonmatches (requiring a "no" response). The N-back blocks were counterbalanced and trial sequence was the same for all participants. The maximum score for each condition was 81, 72, 63, respectively. Performance was calculated as an error-adjusted discrimination score by subtracting the proportion of false alarms (i.e., a wrong answer judged to be correct, or, in other terms, answering Yes, when the correct answer is No) from the proportion of correct hits (i.e., answering Yes when the correct answer is Yes).

PET processing

PET data obtained with [^{11}C]SCH23390 was processed with the following steps: To estimate receptor availability (i.e., D1DR) in targeted regions, binding potential relative to non-displaceable binding in a reference region (BP_{ND}; Innis et al., 2007) was used with cerebellum as reference. The processing of the PET data included correction for head movement by using frame-to-frame image co-registration, and co-registered with T1-weighted MRI data with re-slicing to MRI voxel size using Statistical Parametric Mapping (SPM12: Wellcome Trust Centre for Neuroimaging, http://www.fil.ion.ucl.ac.uk/spm/). To model the regional time-activity course (TAC) data we used simplified reference tissue model (SRTM; Lammertsma & Hume, 1996).

MRI processing

Quantitative susceptibility mapping. Approximation of iron content was inferred from susceptibility values derived from QSM images. Morphology-enabled dipole inversion (MEDI; T. Liu et al., 2011) is a method for QSM estimation that selects the solution that minimizes the discrepancy in the number of voxels belonging to edges between the susceptibility image and the magnitude image. Here, we used the recommended nonlinear variant of MEDI proposed by Liu et al.(2013). Initially, the total field map was estimated from the complex meGRE images by performing a nonlinear least square fitting on a voxel-by-voxel basis. The resulting frequency map was then spatially unwrapped using a guided region-growing unwrapping algorithm (Xu & Cumming, 1999). The background fields, the superimposed field contributions that are not caused by the sources inside the brain and mainly generated by air-tissue interference, were eliminated using a nonparametric technique based on Projection onto Dipole Fields (PDF: Liu et al., 2011). Finally, the corrected frequency map was used as input for the field-to-source inverse problem to calculate susceptibility maps. The MEDI Toolbox (http://weill.cornell.edu/mri/pages/qsm.html) was used to calculate QSM images.

Due to the singularity of dipole kernel at the centre of k-space, the generated QSM images contain relative susceptibility values, which may not necessarily be comparable across subjects. To address this issue, a region of the corticospinal tract was selected as a zero-reference region due to its resilience to age-related degeneration (de Groot et al., 2015) and stable susceptibility across adulthood (Li et al., 2014). Using white-matter areas as reference regions has previously been recommended due to their low standard deviations of susceptibility, indicating low inter-subject variation similar (Straub et al., 2017) or even lower than CSF (Deistung et al., 2013). The process of zero-referencing is described in detail by Garzón and colleagues (2017).

Automated segmentation of cortical and deep gray-matter structures was performed with the Freesurfer image analysis suite — version 6 (http://surfer.nmr.mgh.harva rd.edu/) using T1-weighted images (Fischl et al., 2002; Fischl, Salat, et al., 2004; Fischl, Van Der Kouwe, et al., 2004).

Next, QSM and the segmentation results were resampled to the native structural space. Then, statistics including average and standard deviation were computed on the QSM maps. We merged segmented rostral and caudal middle frontal regions from the left and right hemispheres to form DLPFC (Fig. 1A), and the left and right caudate and putamen to form striatum (supplementary materials Fig. 1A).

Prior to computing statistics on the QSM maps, the boundary of segmentations was eroded by one voxel, and a fraction (15%) of the most extreme values was removed to avoid the influence of high signal from neighbouring vessels and obtain more robust estimates (Garzón et al., 2017).

Functional MRI analyses. Pre-processing of the fMRI data, performed in SPM12 software, included slice-timing correction and motion correction by unwarping and re-alignment to the first image of each volume. The fMRI volumes were then normalized to a sample-specific template generated using Diffeomorphic Anatomical Registration using Exponentiated Lie algebra (DARTEL: Ashburner, 2007), affine alignment to MNI standard space, and spatial smoothing with a 6-mm full width at half maximum (FWHM) Gaussian kernel (voxel size = $2 \times 2 \times 2$ mm^3).

The pre-processed fMRI data were analysed with spatiotemporal PLS (McIntosh et al., 2004; McIntosh & Lobaugh, 2004) to assess the BOLD association with iron, D1DR, and age across the three experimental WM conditions (1-, 2-, and 3-back). PLS determines time-varying distributed patterns of neural activity as a function of experimental variables (1-, 2-, and 3-back) and regional iron and D1DR. This technique allows for the identification of patterns/networks, which reflect association changes across all regions of the brain simultaneously, rather than assemblies of independent regions, thus ruling out the need for multiple-comparison correction. A detailed description of spatiotemporal PLS analysis for fMRI data has been given in previous reports (Garrett et al., 2010; Grady & Garrett, 2014; Salami et al., 2010, 2012, 2014).

The onset of each stimulus within each block of images (1-, 2-, and 3-back) was averaged across blocks for each condition. A cross-block correlation matrix was computed as the correlation between neural activity across experimental conditions (1-, 2-, and 3-back) and variables of interest (age, D1DR, iron)

387 across different regions. Then, the correlation matrix was decomposed using singular value
388 decomposition (SVD), to identify a set of orthogonal latent variables (LVs) representing linear
389 combinations of the original variables:

390 $SVD_{CORR} = USV'$

391 This decomposition produces a left singular vector of regional susceptibility weights (U), a right singular
392 vector of BOLD weights (V), and a diagonal matrix of singular values (S). This analysis produces
393 orthogonal LVs that optimally represent relations between the variables of interest (age, D1DR, iron)
394 and BOLD. Note that PLS is not mathematically susceptible to collinearity similar to the multiple
395 regression approach (Leibovitch et al., 1999). Each LV contains a spatial pattern exhibiting the brain
396 regions whose activity shows the strongest simultaneous relations to the input variables. To obtain a
397 summary measure of each participant's expression of a particular LV pattern, subject-specific "brain
398 scores" are computed by multiplying each voxel's (i) weight (V) from each LV (j) by the BOLD value in
399 that voxel for person (m), and summing over all (n) brain voxels:

400 $$\sum_{i=l}^{n} \mathrm{v}_{ij}\mathrm{BOLD}_{im}$$

401

402 Taken together, a brain score represents the degree to which each subject contributes to the
403 multivariate spatial pattern captured by a latent variable.

404 The statistical significance of each LV was assessed using permutation testing. This procedure involved
405 reshuffling the rows of the data matrix and recalculating the LVs of the reshuffled matrix using the
406 same SVD approach. The number of times a permuted singular value exceeds the original singular value
407 yields the probability of significance of the original LV (McIntosh et al., 1996). In the present study,
408 1000 permutations were performed. In addition, the stability of voxel saliencies contributing to each
409 LV was determined with bootstrap estimation of standard errors (SEs), using 1000 bootstrap samples

(Efron & Tibshirani, 1986). The Bootstrap Ratio (BSR: the ratio between voxel saliences and estimated SEs) was computed and voxels with BSR > 3.29 (similar to a Z-score of 3.29, corresponding to p = 0.001) were considered reliable. All reliable clusters comprised contiguous voxels, with a distance between clusters of at least 10 mm. Moreover, the upper and lower percentiles of the bootstrap distribution were used to generate 95% confidence intervals (CIs) around the correlation scores to facilitate interpretation (McIntosh & Lobaugh, 2004). For instance, a significant difference between correlation scores in different conditions is indicated by non-overlapping CIs. Similarly, brain or correlation scores were considered unreliable when CIs overlapped with zero.

PLS uses all conditions of an experiment and variables of interest at once, thus offering an additional dimension by simultaneously considering both similarities and differences across the experimental variables. If the variables of interest (i.e., age, iron content, D1DR) are similarly related to brain regions, PLS reveals a pattern with reliable loadings (with/without quantitative differences) for all variables. If a single variable dominates the pattern, PLS should reveal a reliable loading for that variable only. Alternatively, if different variables (e.g., D1DR and iron) differentially modulate BOLD response (e.g., Load-dependent effects of dopamine on BOLD as shown in Salami et al., (2019) versus load-independent effect of iron on BOLD shown in Salami et al., 2021), PLS may reveal two distinctive networks.

Additional statistical analyses

To assess age-effects on cognitive performance, a multivariate analysis of covariance (MANCOVA) was conducted with WM load-conditions as dependent variables and age-groups (younger vs. middle-aged vs. older) as between-subjects factors. Follow-up independent t-tests were conducted to assess significant differences between age groups. To assess the relationship between iron content and D1DR, we conducted partial correlation analyses for each region of interest with iron content and D1DR as dependent variables, controlling for age. As control analyses, we performed the same analyses but included sex, education, and regional grey-matter volume as covariates.

435

436 **Author credit statement**

437 AS and GK designed the study. JG, GK and AS performed the research. JG, GK, AS, JJ, FF, GP, MA, and
438 BAP analysed and interpreted the data. JG, FF, GK, AS, GP, and BAP wrote the manuscript which was
439 edited by all authors.

440 **Acknowledgement**

441 We thank the staff of the DyNAMiC project, Frida Magnusson and Emma Simonsson, staff at MRI and
442 PET labs at Umeå University Hospital, and all our participants. We also thank Robin Pedersen for his
443 contribution with the figures.

444 **Conflict of interest**

445 The authors declare no conflict of interest.

446 **Ethics approval**

447 This study was approved by the Regional Ethical board and the local Radiation Safety Committee in
448 Umeå, Sweden.

449 **Data availability statement**

450 Data from the DyNAMiC project cannot be made publicly available due to ethical and legal restrictions.
451 However, access to these original data may be available upon request from the corresponding author.

5. References

Andrews-Hanna, J. R., Snyder, A. Z., Vincent, J. L., Lustig, C., Head, D., Raichle, M. E., & Buckner, R. L. (2007). Disruption of Large-Scale Brain Systems in Advanced Aging. *Neuron*, *56*(5), 924–935. https://doi.org/10.1016/j.neuron.2007.10.038

Ashburner, J. (2007). A fast diffeomorphic image registration algorithm. *NeuroImage*, *38*(1), 95–113. https://doi.org/10.1016/j.neuroimage.2007.07.007

Bäckman, L., Ginovart, N., Dixon, R. A., Wahlin, T. B. R., Wahlin, Å., Halldin, C., & Farde, L. (2000). Age-related cognitive deficits mediated by changes in the striatal dopamine system. *American Journal of Psychiatry*, *157*(4), 635–637. https://doi.org/10.1176/appi.ajp.157.4.635

Bäckman, L., Karlsson, S., Fischer, H., Karlsson, P., Brehmer, Y., Rieckmann, A., MacDonald, S. W. S., Farde, L., & Nyberg, L. (2011). Dopamine D1 receptors and age differences in brain activation during working memory. *Neurobiology of Aging*, *32*(10), 1849–1856. https://doi.org/10.1016/j.neurobiolaging.2009.10.018

Bäckman, L., Nyberg, L., Lindenberger, U., Li, S. C., & Farde, L. (2006). The correlative triad among aging, dopamine, and cognition: Current status and future prospects. *Neuroscience and Biobehavioral Reviews*, *30*(6), 791–807. https://doi.org/10.1016/j.neubiorev.2006.06.005

Cappell, K. A., Gmeindl, L., & Reuter-Lorenz, P. A. (2010). Age differences in prefontal recruitment during verbal working memory maintenance depend on memory load. *Cortex*, *46*(4), 462–473. https://doi.org/10.1016/j.cortex.2009.11.009

Cass, W. A., Grondin, R., Andersen, A. H., Zhang, Z., Hardy, P. A., Hussey-Andersen, L. K., Rayens, W. S., Gerhardt, G. A., & Gash, D. M. (2007). Iron accumulation in the striatum predicts aging-related decline in motor function in rhesus monkeys. *Neurobiology of Aging*, *28*(2), 258–271. https://doi.org/10.1016/j.neurobiolaging.2005.12.010

Cools, R., & D'Esposito, M. (2011). Inverted-U–Shaped Dopamine Actions on Human Working Memory and Cognitive Control. *Biological Psychiatry*, *69*(12), e113–e125. https://doi.org/https://doi.org/10.1016/j.biopsych.2011.03.028

Daugherty, A. M., Haacke, E. M., & Raz, N. (2015). Striatal iron content predicts its shrinkage and changes in verbal working memory after two years in healthy adults. *Journal of Neuroscience*, *35*(17), 6731–6743. https://doi.org/10.1523/JNEUROSCI.4717-14.2015

Daugherty, A. M., & Raz, N. (2015). Appraising the Role of Iron in Brain Aging and Cognition: Promises and Limitations of MRI Methods. *Neuropsychology Review*, *25*(3), 272–287. https://doi.org/10.1007/s11065-015-9292-y

Daugherty, A. M., & Raz, N. (2016). Accumulation of iron in the putamen predicts its shrinkage in healthy older adults: A multi-occasion longitudinal study. *NeuroImage*, *128*(1), 11–20. https://doi.org/10.1016/j.neuroimage.2015.12.045

de Groot, M., Ikram, M. A., Akoudad, S., Krestin, G. P., Hofman, A., Lugt, A., Niessen, W. J., & Vernooij, M. W. (2015). Tract-specific white matter degeneration in aging: The Rotterdam Study. *Alzheimer's & Dementia*, *11*(3), 321–330. https://doi.org/10.1016/j.jalz.2014.06.011

Deistung, A., Schäfer, A., Schweser, F., Biedermann, U., Turner, R., & Reichenbach, J. R. (2013). Toward in vivo histology: A comparison of quantitative susceptibility mapping (QSM) with magnitude-, phase-, and R2*-imaging at ultra-high magnetic field strength. *NeuroImage*, *65*, 299–314. https://doi.org/10.1016/j.neuroimage.2012.09.055

Dichtl, S., Haschka, D., Nairz, M., Seifert, M., Volani, C., Lutz, O., & Weiss, G. (2018). Dopamine

promotes cellular iron accumulation and oxidative stress responses in macrophages. *Biochemical Pharmacology*, *148*, 193–201. https://doi.org/10.1016/j.bcp.2017.12.001

Efron, B., & Tibshirani, R. (1986). Bootstrap Methods for Standard Errors, Confidence Intervals, and Other Measures of Statistical Accuracy. *Statistical Science*, *1*(1), 15–51. https://doi.org/10.1214/ss/1177013815

Erikson, K. M., Jones, B. C., Hess, E. J., Zhang, Q., & Beard, J. L. (2001). Iron deficiency decreases dopamine D1 and D2 receptors in rat brain. *Pharmacology Biochemistry and Behavior*, *69*(3–4), 409–418. https://doi.org/10.1016/S0091-3057(01)00563-9

Fischer, H., Nyberg, L., Karlsson, S., Karlsson, P., Brehmer, Y., Rieckmann, A., MacDonald, S. W. S., Farde, L., & Bäckman, L. (2010). Simulating Neurocognitive Aging: Effects of a Dopaminergic Antagonist on Brain Activity During Working Memory. *Biological Psychiatry*, *67*(6), 575–580. https://doi.org/10.1016/j.biopsych.2009.12.013

Fischl, B., Salat, D. H., Busa, E., Albert, M., Dieterich, M., Haselgrove, C., Van Der Kouwe, A., Killiany, R., Kennedy, D., Klaveness, S., Montillo, A., Makris, N., Rosen, B., & Dale, A. M. (2002). Whole brain segmentation: Automated labeling of neuroanatomical structures in the human brain. *Neuron*, *33*(3), 341–355. https://doi.org/10.1016/S0896-6273(02)00569-X

Fischl, B., Salat, D. H., Van Der Kouwe, A. J. W., Makris, N., Ségonne, F., Quinn, B. T., & Dale, A. M. (2004). Sequence-independent segmentation of magnetic resonance images. *NeuroImage*, *23*(SUPPL. 1), 69–84. https://doi.org/10.1016/j.neuroimage.2004.07.016

Fischl, B., Van Der Kouwe, A., Destrieux, C., Halgren, E., Ségonne, F., Salat, D. H., Busa, E., Seidman, L. J., Goldstein, J., Kennedy, D., Caviness, V., Makris, N., Rosen, B., & Dale, A. M. (2004). Automatically Parcellating the Human Cerebral Cortex. *Cerebral Cortex*, *14*(1), 11–22. https://doi.org/10.1093/cercor/bhg087

Garrett, D. D., Kovacevic, N., McIntosh, A. R., & Grady, C. L. (2010). Blood oxygen level-dependent signal variability is more than just noise. *Journal of Neuroscience*, *30*(14), 4914–4921. https://doi.org/10.1523/JNEUROSCI.5166-09.2010

Garzón, B., Sitnikov, R., Bäckman, L., & Kalpouzos, G. (2017). Can transverse relaxation rates in deep gray matter be approximated from functional and T2-weighted FLAIR scans for relative brain iron quantification? *Magnetic Resonance Imaging*, *40*, 75–82. https://doi.org/10.1016/j.mri.2017.04.005

Gorbach, T., Pudas, S., Lundquist, A., Orädd, G., Josefsson, M., Salami, A., de Luna, X., & Nyberg, L. (2017). Longitudinal association between hippocampus atrophy and episodic-memory decline. *Neurobiology of Aging*, *51*, 167–176. https://doi.org/10.1016/j.neurobiolaging.2016.12.002

Grady, C. L., & Garrett, D. D. (2014). Understanding variability in the BOLD signal and why it matters for aging. *Brain Imaging and Behavior*, *8*(2), 274–283. https://doi.org/10.1007/s11682-013-9253-0

Gustavsson, J., Papenberg, G., Falahati, F., Laukka, E. J., & Kalpouzos, G. (2022). Contributions of the Catechol-O-Methyltransferase Val158Met Polymorphism to Changes in Brain Iron Across Adulthood and Their Relationships to Working Memory. *Frontiers in Human Neuroscience*, *16*. https://doi.org/10.3389/fnhum.2022.838228

Haider, L. (2015). Inflammation, Iron, Energy Failure, and Oxidative Stress in the Pathogenesis of Multiple Sclerosis. *Oxidative Medicine and Cellular Longevity*, *2015*(3), 1–10. https://doi.org/10.1155/2015/725370

Hald, A., & Lotharius, J. (2005). Oxidative stress and inflammation in Parkinson's disease: Is there a

causal link? *Experimental Neurology*, *193*(2), 279–290. https://doi.org/10.1016/j.expneurol.2005.01.013

Hallgren, B., & Sourander, P. (1958). The Effect of Age on the Non-Haemin Iron in the Human Brain. *Journal of Neurochemistry*, *3*(1), 41–51. https://doi.org/10.1111/j.1471-4159.1958.tb12607.x

Hare, D. J., & Double, K. L. (2016). Iron and dopamine: A toxic couple. *Brain*, *139*(4), 1026–1035. https://doi.org/10.1093/brain/aww022

He, Y., Thong, P. S., Lee, T., Leong, S. ., Mao, B. Y., Dong, F., & Watt, F. (2003). Dopaminergic cell death precedes iron elevation in MPTP-injected monkeys. *Free Radical Biology and Medicine*, *35*(5), 540–547. https://doi.org/doi.org/10.1016/j.neurobiolaging.2005.12.010

Innis, R. B., Cunningham, V. J., Delforge, J., Fujita, M., Gjedde, A., Gunn, R. N., Holden, J., Houle, S., Huang, S.-C., Ichise, M., Iida, H., Ito, H., Kimura, Y., Koeppe, R. A., Knudsen, G. M., Knuuti, J., Lammertsma, A. A., Laruelle, M., Logan, J., … Carson, R. E. (2007). Consensus Nomenclature for in vivo Imaging of Reversibly Binding Radioligands. *Journal of Cerebral Blood Flow & Metabolism*, *27*(9), 1533–1539. https://doi.org/10.1038/sj.jcbfm.9600493

Johansson, J., Nordin, K., Pedersen, R., Karalija, N., Papenberg, G., Andersson, M., Korkki, S. M., Riklund, K., Guitart-Masip, M., Rieckmann, A., Bäckman, L., Nyberg, L., & Salami, A. (2022). Bi-phasic patterns of age-related differences in dopamine D1 receptors across the adult lifespan. *BioRxiv*, 1–35. https://doi.org/10.1101/2022.05.24.493225

Kalpouzos, G. (2018). Brain iron accumulation, and motor and cognitive decline in normal aging. *Revue de Neuropsychologie*, *10*(3), 205. https://doi.org/10.3917/rne.103.0205

Kalpouzos, G., Garzón, B., Sitnikov, R., Heiland, C., Salami, A., Persson, J., & Bäckman, L. (2017). Higher Striatal Iron Concentration is Linked to Frontostriatal Underactivation and Poorer Memory in Normal Aging. *Cerebral Cortex*, *27*(6), 3427–3436. https://doi.org/10.1093/cercor/bhx045

Karrer, T. M., Josef, A. K., Mata, R., Morris, E. D., & Samanez-Larkin, G. R. (2017). Reduced dopamine receptors and transporters but not synthesis capacity in normal aging adults: a meta-analysis. *Neurobiology of Aging*, *57*, 36–46. https://doi.org/10.1016/j.neurobiolaging.2017.05.006

Kaur, D., Yantiri, F., Rajagopalan, S., Kumar, J., Mo, J. Q., Boonplueang, R., Viswanath, V., Jacobs, R., Yang, L., Beal, M. F., DiMonte, D., Volitaskis, I., Ellerby, L., Cherny, R. A., Bush, A. I., & Andersen, J. K. (2003). Genetic or Pharmacological Iron Chelation Prevents MPTP-Induced Neurotoxicity In Vivo. *Neuron*, *37*(6), 899–909. https://doi.org/10.1016/S0896-6273(03)00126-0

Lammertsma, A. A., & Hume, S. P. (1996). Simplified Reference Tissue Model for PET Receptor Studies. *NeuroImage*, *4*(3), 153–158. https://doi.org/10.1006/nimg.1996.0066

Landau, S. M., Lal, R., O'Neil, J. P., Baker, S., & Jagust, W. J. (2009). Striatal dopamine and working memory. *Cerebral Cortex*, *19*(2), 445–454. https://doi.org/10.1093/cercor/bhn095

Langkammer, C., Schweser, F., Krebs, N., Deistung, A., Goessler, W., Scheurer, E., Sommer, K., Reishofer, G., Yen, K., Fazekas, F., Ropele, S., & Reichenbach, J. R. (2012). Quantitative susceptibility mapping (QSM) as a means to measure brain iron? A post mortem validation study. *NeuroImage*, *62*(3), 1593–1599. https://doi.org/10.1016/j.neuroimage.2012.05.049

Larsen, B., Olafsson, V., Calabro, F., Laymon, C., Tervo-Clemmens, B., Campbell, E., Minhas, D., Montez, D., Price, J., & Luna, B. (2020). Maturation of the human striatal dopamine system revealed by PET and quantitative MRI. *Nature Communications*, *11*(1), 1–10. https://doi.org/10.1038/s41467-020-14693-3

582 Leibovitch, F. S., Black, S. E., Caldwell, C. B., McIntosh, A. R., Ehrlich, L. E., & Szalai, J. P. (1999). Brain
583 SPECT imaging and left hemispatial neglect covaried using partial least squares: The sunnybrook
584 stroke study. *Human Brain Mapping*, *7*(4), 244–253. https://doi.org/10.1002/(SICI)1097-
585 0193(1999)7:4<244::AID-HBM3>3.0.CO;2-K

586 Li, W., Wu, B., Batrachenko, A., Bancroft-Wu, V., Morey, R. A., Shashi, V., Langkammer, C., De Bellis,
587 M. D., Ropele, S., Song, A. W., & Liu, C. (2014). Differential developmental trajectories of
588 magnetic susceptibility in human brain gray and white matter over the lifespan. *Human Brain*
589 *Mapping*, *35*(6), 2698–2713. https://doi.org/10.1002/hbm.22360

590 Lillig, C. H., Berndt, C., & Holmgren, A. (2008). Glutaredoxin systems. *Biochimica et Biophysica Acta -*
591 *General Subjects*, *1780*(11), 1304–1317. https://doi.org/10.1016/j.bbagen.2008.06.003

592 Liu, T., Liu, J., De Rochefort, L., Spincemaille, P., Khalidov, I., Ledoux, J. R., & Wang, Y. (2011).
593 Morphology enabled dipole inversion (MEDI) from a single-angle acquisition: Comparison with
594 COSMOS in human brain imaging. *Magnetic Resonance in Medicine*, *66*(3), 777–783.
595 https://doi.org/10.1002/mrm.22816

596 Liu, T., Wisnieff, C., Lou, M., Chen, W., Spincemaille, P., & Wang, Y. (2013). Nonlinear formulation of
597 the magnetic field to source relationship for robust quantitative susceptibility mapping.
598 *Magnetic Resonance in Medicine*, *69*(2), 467–476. https://doi.org/10.1002/mrm.24272

599 Liu, Z., Zhai, X. R., Du, Z. S., Xu, F. F., Huang, Y., Wang, X. Q., Qiu, Y. H., & Peng, Y. P. (2021). Dopamine
600 receptor D2 on CD4+ T cells is protective against neuroinflammation and neurodegeneration in
601 a mouse model of Parkinson's disease. *Brain, Behavior, and Immunity*, *98*(April), 110–121.
602 https://doi.org/10.1016/j.bbi.2021.08.220

603 Mattay, V. S., Fera, F., Tessitore, A., Hariri, A. R., Berman, K. F., Das, S., Meyer-Lindenberg, A.,
604 Goldberg, T. E., Callicott, J. H., & Weinberger, D. R. (2006). Neurophysiological correlates of age-
605 related changes in working memory capacity. *Neuroscience Letters*, *392*(1–2), 32–37.
606 https://doi.org/10.1016/j.neulet.2005.09.025

607 Mazhar, M., Din, A. U., Ali, H., Yang, G., Ren, W., Wang, L., Fan, X., & Yang, S. (2021). Implication of
608 ferroptosis in aging. *Cell Death Discovery*, *7*(1), 1–9. https://doi.org/10.1038/s41420-021-
609 00553-6

610 McCann, H., Cartwright, H., & Halliday, G. M. (2016). Neuropathology of α-synuclein propagation and
611 braak hypothesis. *Movement Disorders*, *31*(2), 152–160. https://doi.org/10.1002/mds.26421

612 McIntosh, A. R., Bookstein, F. L., Haxby, J. V., & Grady, C. L. (1996). Spatial pattern analysis of
613 functional brain images using partial least squares. *NeuroImage*, *3*(3 I), 143–157.
614 https://doi.org/10.1006/nimg.1996.0016

615 McIntosh, A. R., Chau, W. K., & Protzner, A. B. (2004). Spatiotemporal analysis of event-related fMRI
616 data using partial least squares. *NeuroImage*, *23*(2), 764–775.
617 https://doi.org/10.1016/j.neuroimage.2004.05.018

618 McIntosh, A. R., & Lobaugh, N. J. (2004). Partial least squares analysis of neuroimaging data:
619 Applications and advances. *NeuroImage*, *23*(SUPPL. 1), 250–263.
620 https://doi.org/10.1016/j.neuroimage.2004.07.020

621 Mills, E., Dong, X. P., Wang, F., & Xu, H. (2010). Mechanisms of brain iron transport: Insight into
622 neurodegeneration and CNS disorders. *Future Medicinal Chemistry*, *2*(1), 51–64.
623 https://doi.org/10.4155/fmc.09.140

624 Nordin, K., Gorbach, T., Pedersen, R., Lundmark, V. P., Johansson, J., Andersson, M., Mcnulty, C.,
625 Riklund, K., Wåhlin, A., Papenberg, G., Kalpouzos, G., Bäckman, L., & Salami, A. (2022).

626 DyNAMiC : A prospective longitudinal study of dopamine and brain connectomes : A new
627 window into cognitive aging. *Journal of Neuroscience Research*, *January*, 1–25.
628 https://doi.org/10.1002/jnr.25039

629 Nyberg, L., Andersson, M., Forsgren, L., Jakobsson-Mo, S., Larsson, A., Marklund, P., Nilsson, L. G.,
630 Riklund, K., & Bäckman, L. (2009). Striatal dopamine D2 binding is related to frontal BOLD
631 response during updating of long-term memory representations. *NeuroImage*, *46*(4), 1194–
632 1199. https://doi.org/10.1016/j.neuroimage.2009.03.035

633 Nyberg, L., Andersson, M., Kauppi, K., Lundquist, A., Persson, J., Pudas, S., & Nilsson, L.-G. (2014).
634 Age-related and Genetic Modulation of Frontal Cortex Efficiency. *Journal of Cognitive*
635 *Neuroscience*, *26*(4), 746–754. https://doi.org/10.1162/jocn_a_00521

636 Nyberg, L., Dahlin, E., Stigsdotter Neely, A., & BÄckman, L. (2009). Neural correlates of variable
637 working memory load across adult age and skill: Dissociative patterns within the fronto-parietal
638 network: Cognition and Neurosciences. *Scandinavian Journal of Psychology*, *50*(1), 41–46.
639 https://doi.org/10.1111/j.1467-9450.2008.00678.x

640 Ortega, R., Cloetens, P., Devès, G., Carmona, A., & Bohic, S. (2007). Iron storage within dopamine
641 neurovesicles revealed by chemical nano-imaging. *PLoS ONE*, *2*(9).
642 https://doi.org/10.1371/journal.pone.0000925

643 Poetini, M. R., Araujo, S. M., Trindade de Paula, M., Bortolotto, V. C., Meichtry, L. B., Polet de
644 Almeida, F., Jesse, C. R., Kunz, S. N., & Prigol, M. (2018). Hesperidin attenuates iron-induced
645 oxidative damage and dopamine depletion in Drosophila melanogaster model of Parkinson's
646 disease. *Chemico-Biological Interactions*, *279*(September 2017), 177–186.
647 https://doi.org/10.1016/j.cbi.2017.11.018

648 Reuter-Lorenz, P. A., & Cappell, K. A. (2008). Neurocognitive aging and the compensation hypothesis.
649 *Current Directions in Psychological Science*, *17*(3), 177–182. https://doi.org/10.1111/j.1467-
650 8721.2008.00570.x

651 Rieckmann, A., Karlsson, S., Karlsson, P., Brehmer, Y., Fischer, H., Farde, L., Nyberg, L., & Bäckman, L.
652 (2011). Dopamine D1 receptor associations within and between dopaminergic pathways in
653 younger and elderly adults: Links to cognitive performance. *Cerebral Cortex*, *21*(9), 2023–2032.
654 https://doi.org/10.1093/cercor/bhq266

655 Rodrigue, K. M., Daugherty, A. M., Foster, C. M., & Kennedy, K. M. (2020). Striatal iron content is
656 linked to reduced fronto-striatal brain function under working memory load. *NeuroImage*,
657 *210*(October 2019), 116544. https://doi.org/10.1016/j.neuroimage.2020.116544

658 Salami, A., Avelar-Pereira, B., Garzón, B., Sitnikov, R., & Kalpouzos, G. (2018). Functional coherence of
659 striatal resting-state networks is modulated by striatal iron content. *NeuroImage*, *183*(April),
660 495–503. https://doi.org/10.1016/j.neuroimage.2018.08.036

661 Salami, A., Eriksson, J., Kompus, K., Habib, R., Kauppi, K., & Nyberg, L. (2010). Characterizing the
662 neural correlates of modality-specific and modality-independent accessibility and availability
663 signals in memory using partial-least squares. *NeuroImage*, *52*(2), 686–698.
664 https://doi.org/10.1016/j.neuroimage.2010.04.195

665 Salami, A., Eriksson, J., & Nyberg, L. (2012). Opposing effects of aging on large-scale Brain systems for
666 memory encoding and cognitive control. *Journal of Neuroscience*, *32*(31), 10749–10757.
667 https://doi.org/10.1523/JNEUROSCI.0278-12.2012

668 Salami, A., Garrett, D. D., Wåhlin, A., Rieckmann, A., Papenberg, G., Karalija, N., Jonasson, L.,
669 Andersson, M., Axelsson, J., Johansson, J., Riklund, K., Lövdén, M., Lindenberger, U., Bäckman,

L., & Nyberg, L. (2019). Dopamine D 2/3 binding potential modulates neural signatures of working memory in a load-dependent fashion. *Journal of Neuroscience*, *39*(3), 537–547. https://doi.org/10.1523/JNEUROSCI.1493-18.2018

Salami, A., Papenberg, G., Sitnikov, R., Laukka, E. J., Persson, J., & Kalpouzos, G. (2021). Elevated Neuroinflammation Contributes to the Deleterious Impact of Iron Overload on Brain Function in Aging. *NeuroImage*, *230*(August 2020), 117792. https://doi.org/10.1016/j.neuroimage.2021.117792

Salami, A., Rieckmann, A., Fischer, H., & Bäckman, L. (2014). A multivariate analysis of age-related differences in functional networks supporting conflict resolution. *NeuroImage*, *86*, 150–163. https://doi.org/10.1016/j.neuroimage.2013.08.002

Salthouse, T. (2012). Consequences of age-related cognitive declines. Annual review of psychology. *Annu Rev Psychol.*, *63*, 201-226. https://doi.org/10.1146/annurev-psych-120710-100328.Consequences

Schneider-Garces, N. J., Gordon, B. A., Brumback-Peltz, C. R., Shin, E., Lee, Y., Sutton, B. P., Maclin, E. L., Gratton, G., & Fabiani, M. (2010). Span, CRUNCH, and beyond: Working memory capacity and the aging brain. *Journal of Cognitive Neuroscience*, *22*(4), 655–669. https://doi.org/10.1162/jocn.2009.21230

Shao, W., Zhang, S., Tang, M., Zhang, X., Zhou, Z., Yin, Y., Zhou, Q., Huang, Y., Liu, Y., Wawrousek, E., Chen, T., Li, S., Xu, M., Zhou, J., Hu, G., & Zhou, J. (2013). Suppression of neuroinflammation by astrocytic dopamine D2 receptors via αB-crystallin. *Nature*, *494*, 90–94. https://doi.org/https://doi.org/10.1038/nature11748

Shohamy, D., & Adcock, R. A. (2010). Dopamine and adaptive memory. *Trends in Cognitive Sciences*, *14*(10), 464–472. https://doi.org/10.1016/j.tics.2010.08.002

Spence, H., McNeil, C. J., & Waiter, G. D. (2020). The impact of brain iron accumulation on cognition: A systematic review. *PLoS ONE*, *15*(10 October). https://doi.org/10.1371/journal.pone.0240697

Steiger, T. K., Weiskopf, N., & Bunzeck, N. (2016). Iron level and myelin content in the ventral striatum predict memory performance in the aging brain. *Journal of Neuroscience*, *36*(12), 3552–3558. https://doi.org/10.1523/JNEUROSCI.3617-15.2016

Straub, S., Schneider, T. M., Emmerich, J., Freitag, M. T., Ziener, C. H., Schlemmer, H. P., Ladd, M. E., & Laun, F. B. (2017). Suitable reference tissues for quantitative susceptibility mapping of the brain. *Magnetic Resonance in Medicine*, *78*(1), 204–214. https://doi.org/10.1002/mrm.26369

Tabachnick, B., & Fidell, L. (2013). Using Multivariate Statistics. In *Singular Spectrum Analysis* (6th ed.). Pearson. https://doi.org/10.1007/978-1-4757-2514-8_3

Unger, E. L., Bianco, L. E., Jones, B. C., Allen, R. P., & Earley, C. J. (2014). Low brain iron effects and reversibility on striatal dopamine dynamics. *Experimental Neurology*, *261*, 462–468. https://doi.org/10.1016/j.expneurol.2014.06.023

Ward, R. J., Zucca, F. A., Duyn, J. H., Crichton, R. R., & Zecca, L. (2014). The role of iron in brain ageing and neurodegenerative disorders. *The Lancet Neurology*, *13*(10), 1045–1060. https://doi.org/10.1016/S1474-4422(14)70117-6

Xu, W., & Cumming, I. (1999). A region-growing algorithm for InSAR phase unwrapping. *IEEE Transactions on Geoscience and Remote Sensing*, *37*(1), 124–134. https://doi.org/10.1109/36.739143

Yan, Y., Jiang, W., Liu, L., Wang, X., Ding, C., Tian, Z., & Zhou, R. (2015). Dopamine Controls Systemic

713 Inflammation through Inhibition of NLRP3 Inflammasome. *Cell*, *160*(1–2), 62–73.
714 https://doi.org/10.1016/j.cell.2014.11.047

715 Youdim, M. B. H., Ben-Shachar, D., & Riederer, P. (1993). The possible role of iron in the
716 etiopathology of parkinson's disease. *Movement Disorders*, *8*(1), 1–12.
717 https://doi.org/10.1002/mds.870080102

718 Zecca, L., Youdim, M., Riederer, P., Connor, J. R., & Crichton, R. R. (2004). Iron, brain ageing and
719 neurodegenerative disorders. *Nature Reviews Neuroscience*, *5*(11), 863–873.
720 https://doi.org/10.1038/nrn1537

721 Zhu, J., Hu, Z., Han, X., Wang, D., Jiang, Q., Ding, J., Xiao, M., Wang, C., Lu, M., & Hu, G. (2018).
722 Dopamine D2 receptor restricts astrocytic NLRP3 in fl ammasome activation via enhancing the
723 interaction of β -arrestin2 and NLRP3. *Cell Death & Differentiation*, *25*, 2037–2049.
724 https://doi.org/10.1038/s41418-018-0127-2

725 Zimmerman, M. E., Brickman, A. M., Paul, R. H., Grieve, S. M., Tate, D. F., Gunstad, J., Cohen, R. A.,
726 Aloia, M. S., Williams, L. M., Clark, C. R., Whitford, T. J., & Gordon, E. (2006). The relationship
727 between frontal gray matter volume and cognition varies across the healthy adult lifespan.
728 *American Journal of Geriatric Psychiatry*, *14*(10), 823–833.
729 https://doi.org/10.1097/01.JGP.0000238502.40963.ac

730 Zucca, F. A., Segura-Aguilar, J., Ferrari, E., Muñoz, P., Paris, I., Sulzer, D., Sarna, T., Casella, L., & Zecca,
731 L. (2017). Interactions of iron, dopamine and neuromelanin pathways in brain aging and
732 Parkinson's disease. *Progress in Neurobiology*, *155*(3), 96–119.
733 https://doi.org/10.1016/j.pneurobio.2015.09.012

734